GEOPHYSICS, VOL. 72, NO. 6 (NOVEMBER-DECEMBER 2007); P. T81–T95, 13 FIGS.
10.1190/1.2785046

Grid dispersion and stability criteria of some common finite-element methods for acoustic and elastic wave equations

Jonás D. De Basabe[1] and Mrinal K. Sen[2]

ABSTRACT

Purely numerical methods based on finite-element approximation of the acoustic or elastic wave equation are becoming increasingly popular for the generation of synthetic seismograms. We present formulas for the grid dispersion and stability criteria for some popular finite-element methods (FEM) for wave propagation, namely, classical and spectral FEM. We develop an approach based on a generalized eigenvalue formulation to analyze the dispersive behavior of these FEMs for acoustic or elastic wave propagation that overcomes difficulties caused by irregular node spacing within the element and the use of high-order polynomials, as is the case for spectral FEM. Analysis reveals that for spectral FEM of order four or greater, dispersion is less than 0.2% at four to five nodes per wavelength, and dispersion is not angle dependent. New results can be compared with grid-dispersion results of some classical finite-difference methods (FDM) used for acoustic or elastic wave propagation. Analysis reveals that FDM and classical FEM require a larger sampling ratio than a spectral FEM to obtain results with the same degree of accuracy. The staggered-grid FDM is an efficient scheme, but the dispersion is angle dependent with larger values along the grid axes. On the other hand, spectral FEM of order four or greater is isotropic with small dispersion, making it attractive for simulations with long propagation times.

INTRODUCTION

Two of the most common methods for simulating wave propagation in the earth are the finite-difference method (FDM) and finite-element method (FEM). These methods, along with the boundary integral equations method, can be classified as numerical methods, distinct from the analytic methods for wave propagation. Various numerical schemes based on FDM and FEM are reported in the geophysical literature. Examples of FDM are the standard-grid acoustic (Alterman and Karal, 1968; Alford et al., 1974) and elastic formulations (Kelly et al., 1976), and the staggered-grid formulation (Madariaga, 1976; Virieux, 1984, 1986; Levander, 1988; Graves, 1996; Minkoff, 2002). Examples of FEM include the finite-volume method (Dormy and Tarantola, 1995), the mixed FEM (Cohen and Fauqueux, 2000; Jenkins et al., 2002), the classical FEM (CFEM) (Lysmer and Drake, 1972; Mullen and Belytschko, 1982; Marfurt, 1984), the spectral FEM (SEM) (Seriani and Priolo, 1994; Komatitsch and Vilotte, 1998; Komatitsch and Tromp, 1999; Komatitsch et al., 2005; Cohen, 2002), and the ADER discontinuous Galerkin method (Kaser and Dumbser, 2006; Dumbser and Kaser, 2006; Kaser et al., 2007).

Some of the most common FDMs and FEMs used in seismic modeling are explicit, and thus conditionally stable.[3] Generally in seismology, explicit methods are preferred over implicit ones because they need less computation at each time step and have the same order of accuracy. This has been noted for both FDM (Emerman et al., 1982; Carcione et al., 2002) and FEM (Mulder, 1999; Cohen, 2002). The size of the time step is bounded by a stability criterion which is an important factor affecting the accuracy of the results.

A numerical noise related to grid spacing is dispersion, which has a detrimental effect on accuracy. It occurs because the actual velocity of high-frequency waves in the grid is different from the true velocity. This is called grid dispersion because it is originated by the grid and it can occur even when the physical problem is not dispersive. The error introduced by grid dispersion is dependent on grid spacing and the size of the time step.

The purpose of this paper is to analyze the grid-dispersion properties and establish stability criteria for two of the most common FEMs for wave propagation: the classical FEM (Lysmer and Drake, 1972; Mullen and Belytschko, 1982; Marfurt, 1984) and the spectral FEM Seriani and Priolo, 1994; Komatitsch and Vilotte, 1998; Komatitsch

Manuscript received by the Editor 9 September 2006; revised manuscript received 16 July 2007; published online 31 October 2007.
[1]The University of Texas at Austin, John A. and Katherine G. Jackson School of Geosciences, The Institute for Geophysics and The Institute for Computational Engineering and Sciences, Austin, Texas. E-mail: jonas@ig.utexas.edu.
[2]The University of Texas at Austin, The Institute for Computational Engineering and Sciences, Austin, Texas. E-mail: mrinal@ig.utexas.edu.

[3]A numerical algorithm is stable if the difference between the exact and the numerical solutions remains bounded as the time index increases.

and Tromp, 1999; Komatitsch et al., 2005; Cohen, 2002), each applied to the acoustic and elastic wave equations. Here we will use the term CFEM to mean FEM using quadrilateral elements with equally spaced nodes within the element and exact integration, and SEM as FEM using quadrilateral elements with Gauss-Lobatto nodes and integration rules. Note that in SEM the nodes are not equispaced inside the element; they are given by the quadrature points of the Gauss-Lobatto integration rules. Note also that we will consider the order of CFEM or SEM to be the order of the polynomial in one of the sides of the elements.

It is interesting to note that for some time, the FEM was thought to be an inadequate tool for seismic modeling because it required more operations than FDM at each time step without any gain in accuracy (Marfurt, 1984) and because preliminary analysis showed that it introduced spurious waves (Marfurt, 1990). Regarding this, Cohen (2002) remarked, "This was true when people did not know how to mass-lump and when stiffness matrices required a huge storage in finite-element methods." We note that mass lumping is a technique used in FEM to avoid having to invert a matrix at each time step by diagonalizing it; this is done in SEM without loss of accuracy by using the Gauss-Lobatto nodes and quadrature rules.

SEM, originally developed for fluid dynamics (Patera, 1984), has been successfully applied to elastic wave propagation (Komatitsch and Vilotte, 1998), addressing the efficiency issues and providing better accuracy than FDM with more geometrical flexibility. In the recent past SEM has gained tremendous credibility within the seismological community (Komatitsch and Tromp, 1999; Komatitsch et al., 2005), and it has also been applied to global seismology problems with spherical earth models (Komatitsch et al., 2002).

The success of SEM in seismic modeling has outpaced the analytic validation of the method. The accuracy of the Chebyshev-SEM was investigated empirically by Seriani and Priolo (1994) for the acoustic scheme using the Chebyshev-Gauss-Lobatto nodes and quadrature rules, and they concluded that an average of four to five nodes per wavelength with an eighth-order method eliminates grid dispersion. Although this showed promising results, the Chebyshev-SEM does not lead to mass lumping, and it has been pointed out that it is less accurate than the SEM using Gauss-Lobatto nodes and quadrature rules (Mulder, 1999).

The accuracy of the 1D acoustic SEM scheme was examined by Mulder (1999). He concluded that the error introduced by the spurious, or nonphysical, modes can be neglected and that SEM using Gauss-Lobatto nodes and quadrature rules was more accurate than Chebyshev-SEM or classical FEM. He also analyzed the asymptotic behavior of the grid dispersion. Unfortunately it is not clear how to extend his results to higher dimensions.

On the other hand, Cohen (2002) analyzed the grid dispersion of the 1D, 2D, and 3D acoustic SEM schemes analytically using Gauss-Lobatto nodes and quadrature rules. In his approach, he used an eigenvalue formulation and Taylor-series to get the asymptotic behavior of the grid dispersion. In his results, he showed dispersion curves for the 1D case using second- or third-order methods and various time-stepping schemes. See also the preliminary results in Cohen et al. (1994), Tordjman (1995), and Fauqueux (2003).

As for the elastic CFEM or SEM, there seems to be no grid-dispersion or stability-analysis results available in the literature. This has led geophysicists to set the order of the elements and the grid spacing according to the results available for the acoustic case (Komatitsch et al., 2005; Chaljub et al., 2006).

Here we extend the approach of Cohen (2002) to analyze the acoustic CFEM and SEM schemes of any order and develop a similar approach to analyze the elastic CFEM and SEM schemes of any order. For the lowest-order elements, we use this approach to develop grid-dispersion formulas in closed form, and for the higher-order elements we numerically derive the grid-dispersion curves. We also show the grid-dispersion curves of some classical acoustic and elastic FDM and compare those to the corresponding FEM schemes. Our approach in the acoustic case includes the results of Mullen and Belytschko (1982) for quadrilateral elements and agrees with the empirical results of Seriani and Priolo (1994). Furthermore, we confirm the assumptions in Komatitsch et al. (2005) and Chaljub et al. (2006) on the applicability of grid dispersion and stability criteria of the acoustic case to the elastic case.

The main contribution of this paper is the grid-dispersion analysis of the acoustic and elastic SEM of any order. The grid dispersion of the acoustic SEM has been analyzed before, but only for low-order elements or in 1D; the results that we present in this paper are for the 2D case and are for any order. Moreover, the grid dispersion of the elastic SEM has not been analyzed, despite its popularity for seismic modeling. Nevertheless, we do not provide analytic expressions for the grid dispersion but only a numerical approach (analytic expressions are provided only for the first-order elements). We consider only the second-order finite-difference scheme for the discretization in time, which is the most popular time-stepping scheme in SEM for wave propagation (Komatitsch and Tromp, 1999; Chaljub et al., 2006; Cohen, 2002). Other time-stepping schemes have been proposed for seismic modeling; some of them have been analyzed by Mercerat et al. (2006).

The rest of this paper is organized as follows. In the next section we give the formulations of the wave equation and introduce the notation that we will use as well as the assumptions that we make for the analysis. In the "Finite Elements" section, we introduce some basic finite-element concepts such as the weak formulations of the acoustic and elastic wave equations, and the basis functions. The main contribution of this paper is contained in the "Grid Dispersion and Stability Analysis" section, where we develop the stability and grid-dispersion analysis of CFEM and SEM in a unified approach. In the "Results" section we present the results with accompanying figures. The conclusions are summarized in the "Conclusions" section.

FORMULATIONS OF THE WAVE EQUATION

Various forms of the wave equation are useful in seismic modeling. Examples of this are the acoustic and elastic wave equations. The acoustic wave equation models compressional waves propagating through the domain; it is also known as the pressure formulation or as the scalar wave equation because the dependent variable is pressure, a scalar field. The elastic wave equation models the propagation of compressional and shear waves; it is a more accurate approximation of the propagation of waves in the earth, but it is typically more difficult to solve and computationally more expensive because it needs to be solved for displacement, a vector field. Different versions of the elastic wave equation exist for isotropic, anisotropic, homogeneous, or heterogeneous media. Often an elastic wave equation that incorporates the effects of attenuation is known as a seismic wave equation.

In this analysis we will focus on the acoustic and elastic wave equations. Since these formulations do not model physical dispersion, any observed dispersion is attributed to the numerical scheme.

The acoustic wave equation in a heterogeneous medium is given by

$$\nabla \cdot \left(\frac{1}{\rho} \nabla p \right) - \frac{1}{\lambda} \partial_{tt} p = f \quad \text{in } \Omega \times (0, \tau], \tag{1}$$

with some suitable boundary and initial conditions, where $\nabla = (\partial/\partial x, \partial/\partial z)^T$, $\partial_{tt} = \partial^2/\partial t^2$, $p: \Omega \times (0, \tau] \to \mathbf{R}$ is the pressure, $f: \Omega \to \mathbf{R}$ is the source, $\rho: \Omega \to \mathbf{R}$ is the density, $\lambda: \Omega \to \mathbf{R}$ is the first Lamé parameter, $\Omega \subset \mathbf{R}^2$ is the spatial domain, and $(0, \tau]$ is the time domain. The elastic wave equation in an isotropic heterogeneous medium is given by

$$\nabla((\lambda + \mu) \nabla \cdot \mathbf{u}) + \nabla \cdot (\mu \nabla \mathbf{u}) - \rho \partial_{tt} \mathbf{u} = \mathbf{f}$$

$$\text{in} \quad \Omega \times (0, \tau], \tag{2}$$

where $\mathbf{u}: \Omega \times (0, \tau] \to \mathbf{R}^2$ is the displacement, $\mathbf{f}: \Omega \to \mathbf{R}^2$ is the source, and $\mu: \Omega \to \mathbf{R}$ is the second Lamé parameter.

Because the goal of this analysis is to derive the stability condition and grid-dispersion relations, to have a manageable set of parameters we will make several assumptions about the medium. We will assume that the medium is isotropic, homogeneous, unbounded, and source free. For convenience, these will be referred to as the *simplifying assumptions*. Similar assumptions are always made whenever a plane-wave analysis is sought; see for example Alford et al. (1974), Mullen and Belytschko (1982), Marfurt (1984), Moczo et al. (2000a, b), and Cohen (2002). We emphasize here that in practice these assumptions are not expected to be satisfied, nevertheless the results from an analysis based on these assumptions can provide valuable information to determine the discretization parameters for a numerical experiment.

Under these simplifying assumptions, equation 1 takes the following form

$$\alpha^2 \nabla \cdot \nabla p - \partial_{tt} p = 0, \tag{3}$$

where $\alpha = \sqrt{\lambda/\rho}$ is the acoustic wave velocity. Similarly for equation 2 we have

$$(\alpha^2 - \beta^2) \nabla (\nabla \cdot \mathbf{u}) + \beta^2 \nabla \cdot \nabla \mathbf{u} - \partial_{tt} \mathbf{u} = 0, \tag{4}$$

where $\alpha = \sqrt{(\lambda + 2\mu)/\rho}$ is the compressional wave (P-wave) velocity and $\beta = \sqrt{\mu/\rho}$ is the shear wave (S-wave) velocity.

FINITE ELEMENTS

Acoustic formulation

The first step in a finite-element approximation is to derive the weak, or variational, formulations of equations 3 and 4. The weak formulation of the acoustic wave equation is given by multiplying equation 3 by an arbitrary function v, integrating over the domain and using the divergence theorem to get

$$\alpha^2 \int_\Omega \nabla p \cdot \nabla v dx dz + \partial_{tt} \int_\Omega p v dx dz = 0, \tag{5}$$

where $v: \Omega \to \mathbf{R}$ is a sufficiently smooth function, called the test function in the FEM literature. Equation 5 can be written as a system of ODEs by substituting some basis functions for p and v. Let ϕ_i, $i = 1, 2, \ldots, n$, be a set of piecewise polynomial basis functions defined in the domain Ω (the number of basis functions n depends on the number of nodes; see section below on basis functions). Substituting in equation 5 for p the linear combination of the basis functions

$$p(x, z, t) \approx \sum_{j=1}^{n} P_j(t) \phi_j(x, z), \tag{6}$$

where P_j are the coefficients of the FEM approximation of p, and substituting for v each of the basis functions, we get (using Einstein's summation convention)

$$M_{ij} \partial_{tt} P_j + K_{ij} P_j = 0, \tag{7}$$

where

$$M_{ij} = \int_\Omega \phi_i \phi_j dx dz \quad \text{and} \quad K_{ij} = \alpha^2 \int_\Omega \nabla \phi_i \cdot \nabla \phi_j dx dz. \tag{8}$$

Usually in the FEM literature $\mathbf{M}$ represents the mass matrix and $\mathbf{K}$ represents the stiffness matrix. We will use these names because they are standard in FEM terminology, even though they can be misleading in the wave propagation context since the matrices are not necessarily related to mass or stiffness. The ODE system 7 is called the *continuous in time* or semidiscrete form of equation 3, because it has been discretized in space through the substitution of the basis functions, but the time derivative remains. To obtain a fully discretized form we can substitute the second-order finite-difference operator for the time derivative to obtain

$$M_{ij}(P_j^{l+1} - 2P_j^l + P_j^{l-1}) + \Delta t^2 K_{ij} P_j^l = 0, \tag{9}$$

where the upper index l is the time index and Δt is the size of the time step.

Elastic formulation

Next we follow the same procedure for the elastic wave equation. Taking a dot product of equation 4 with a vector test function, integrating over the domain, and using the divergence theorem, we obtain the weak form of the elastic wave equation, given by

$$(\alpha^2 - \beta^2) \int_\Omega (\nabla \cdot \mathbf{u})(\nabla \cdot \mathbf{v}) dx dz + \beta^2 \int_\Omega \nabla \mathbf{u} : \nabla \mathbf{v} dx dz$$

$$+ \partial_{tt} \int_\Omega \mathbf{u} \cdot \mathbf{v} dx dz = 0, \tag{10}$$

where $\mathbf{v}: \Omega \to \mathbf{R}^2$ is a sufficiently smooth test function and the double dot product is defined as $\mathbf{A}:\mathbf{B} = \sum_{i=1}^{n} \sum_{j=1}^{n} (\mathbf{A})_{ij} (\mathbf{B})_{ij}$ for $\mathbf{A}, \mathbf{B} \in \mathbf{R}^{n \times n}$, where $(\mathbf{A})_{ij}$ and $(\mathbf{B})_{ij}$ are the elements of $\mathbf{A}$ and $\mathbf{B}$.

We can now use the weak formulation of the elastic wave equation to obtain a system of ODEs by substituting some basis functions. In the case of equation 10, the basis functions need to be substituted in each of the two components of $\mathbf{u}$ and $\mathbf{v}$. Substituting for $\mathbf{u}$ the approximation

$$\mathbf{u}(x, z, t) \approx (U_j^x(t) \phi_j(x, z), \quad U_j^z(t) \phi_j(x, z))^T, \tag{11}$$

where U_j^x and U_j^z are the coefficients of the FEM approximations to the horizontal and vertical displacement respectively, and substituting $\mathbf{v} = (\phi_i, 0)^T$ we obtain the following system of equations

$$M_{ij} \partial_{tt} U_j^x + K_{ij}^1 U_j^x + K_{ij}^2 U_j^z = 0. \tag{12}$$

Similarly, if we now substitute $\mathbf{v} = (0, \phi_i)^T$, we obtain

$$M_{ij}\partial_{tt}U_j^z + K_{ij}^3 U_j^x + K_{ij}^4 U_j^z = 0, \tag{13}$$

where the matrices in equations 12 and 13 are given by

$$M_{ij} = \frac{r^2}{\alpha^2}\int_\Omega \phi_i \phi_j dxdz, \tag{14}$$

$$K_{ij}^1 = r^2\int_\Omega \phi_{i,x}\phi_{j,x}dxdz + \int_\Omega \phi_{i,z}\phi_{j,z}dxdz, \tag{15}$$

$$K_{ij}^2 = (r^2 - 1)\int_\Omega \phi_{i,x}\phi_{j,z}dxdz, \tag{16}$$

$$K_{ij}^3 = K_{ji}^2, \tag{17}$$

and

$$K_{ij}^4 = \int_\Omega \phi_{i,x}\phi_{j,x}dxdz + r^2\int_\Omega \phi_{i,z}\phi_{j,z}dxdz, \tag{18}$$

where $r = \alpha/\beta$ is the P- to S-wave velocity ratio. In these equations we use the shorthand notation $\phi_{i,x} = \partial\phi_i/\partial x$ and $\phi_{i,z} = \partial\phi_i/\partial z$. For finite differences in time, we obtain

$$M_{ij}(U_j^{x,l+1} - 2U_j^{x,l} + U_j^{x,l-1}) + \Delta t^2 K_{ij}^1 U_j^{x,l} + K_{ij}^2 U_j^{z,l} = 0 \tag{19}$$

and

$$M_{ij}(U_j^{z,l+1} - 2U_j^{z,l} + U_j^{z,l-1}) + \Delta t^2 K_{ij}^3 U_j^{x,l} + K_{ij}^4 U_j^{z,l} = 0, \tag{20}$$

where l is the time index.

Basis functions

Basis functions, also known as shape functions, play an important role in FEM. A careful selection can lead to an accurate and efficient numerical scheme. In this section we will describe some important characteristics of the basis functions used in CFEM and SEM in a simple setting without trying to be exhaustive; the reader is referred to Hughes (1987) for a more detailed and general presentation.

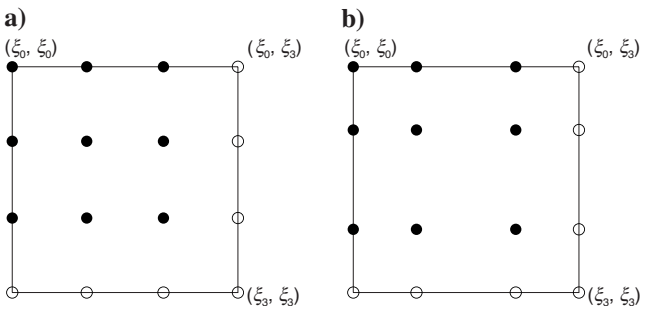

Figure 1. An example of a third-order element in a finite-element mesh using (a) equispaced nodes and (b) the Gauss-Lobatto nodes. The circles represent the nodes, and filled circles represent the κ^2 distinct classes of degrees of freedom (see the "Grid Dispersion and Stability Analysis" section). Note that all the nodes in the mesh can be obtained by translating the set of distinct classes of degrees of freedom by an integer times the element's side (h).

To define the basis functions, we first need a finite-element mesh, given by a set of elements and nodes defined in the domain. The elements are nonoverlapping subdomains that cover the entire domain; for succinctness let us consider rectangular elements (Figure 1). For a basis of order κ we define a grid in one element by defining $\kappa + 1$ nodes in each side of the element. Therefore, the grid will have a total of $(\kappa + 1)^2$ nodes. Clearly, if the elements are rectangular the nodes that are on the sides belong to two elements, and the nodes in the corners to four. In CFEM the nodes are distributed uniformly on each side of the elements, as shown in Figure 1a. However, they also can be distributed nonuniformly. For example, in SEM the nodes are given by the nodes of the Gauss-Lobatto quadrature rule as shown in Figure 1b (Cohen, 2002, see chapters 11 and 12 for details). To develop an approach that applies to CFEM and SEM, we will not assume any particular distribution of the nodes inside the elements in the analysis.

The basis functions in CFEM and in SEM are continuous piecewise polynomial functions with local support, defined to be one at one node and zero on the others. Let us consider an element e with corners at (0,0), (0,1), (1,0), and (1,1). Let $\xi_i, i = 0,1,\ldots,\kappa$, be the nodes on either side of the element (note that $\xi_0 = 0$ and $\xi_\kappa = 1$), and let φ_j, $j = 0,1,\ldots,\kappa$, be the Lagrange polynomials of degree κ that interpolate these nodes, satisfying $\varphi_j(\xi_i) = \delta_{ij}$, where δ_{ij} is Kroneker's delta defined to be one for $i = j$ and zero otherwise. Using these polynomials, the basis functions in element e are given by

$$\phi_q^e(x,z) = \varphi_i(x)\varphi_j(z), \quad i,j = 0,1,\ldots,\kappa, \tag{21}$$

where we have numbered the basis functions with $q = (\kappa + 1)j + i$ instead of the equivalent of using two indices. This notation is useful to reduce the number of indices, for example, in equations 7, 12, and 13. Note that the range of the index is $q = 0,1,\ldots,(\kappa + 1)^2 - 1$ and that, by construction, $\phi_{(\kappa+1)j+i}^e(x_m,z_n) = \varphi_i(x_m)\varphi_j(z_n) = \delta_{im}\delta_{jn}$. When the basis functions are constructed this way, they usually are called tensor product Lagrange basis functions.

Basis functions defined on the entire domain can be constructed using the basis functions defined on element e in equation 21. First note that a basis function can be defined on a node of any element by translating and scaling equation 21. Using these, a global basis function can be built for each node in the domain by fixing them to be zero in all the elements except on those that include the node and putting together all the basis functions defined to be one at that node.

GRID DISPERSION AND STABILITY ANALYSIS

Acoustic case

In this section, we derive grid-dispersion relations for the acoustic CFEM and SEM schemes of any order. The approach is based on a generalized eigenvalue problem that is generally large but can be reduced to order κ^2 by making some assumptions, as we demonstrate here. Furthermore, we will use a generalization of the eigenvalue decomposition introduced by Cohen (2002) to write the eigenvalues of the order κ^2 problem as combinations of the eigenvalues of two order κ problems, making the computation more efficient. Unfortunately we will not be able to write the grid-dispersion relations in closed form except for low-order elements, and in general the grid

dispersion for a given wavenumber and sampling ratio needs to be computed numerically. A method to efficiently compute the grid dispersion and explicit grid-dispersion relations for the first-order CFEM and SEM will be given at the end of this section.

This analysis is based on the von Neumann method (Mitchell and Griffiths, 1980; Hughes, 1987), which assumes a plane-wave propagating through the finite-element domain. Furthermore, we will assume that all the elements in the domain are square with sides h. Note that with this assumption $x_n = h(i + \xi_j)$ and $z_n = h(i + \xi_j)$ with $n = \kappa i + j$ and $0 \le j < \kappa$; thus the nodes are κ-periodic in both directions, $x_{n+\kappa} = x_n + h$ and $z_{n+\kappa} = z_n + h$. Recall that the ξ_j represents the node distribution in one side of the element, and that $\xi_0 = 0$ and $\xi_\kappa = 1$.

If we assume that the solution is a plane wave, then P_j has the following form (no summation over j)

$$P_j(t) = A_j e^{i(\mathbf{k}\cdot\mathbf{x}_j - \omega t)}, \tag{22}$$

where $\mathbf{k}$ is the wavenumber, $\mathbf{x}_j$ contains the jth node coordinates, and A_j is an arbitrary constant. Note that equation 22 represents a plane wave evaluated at the jth node. Substituting equation 22 in equation 7 or 9 we derive the following generalized eigenvalue problem

$$\Lambda M_{ij} P_j = K_{ij} P_j, \tag{23}$$

where M_{ij} and K_{ij} are given in equation 8. The matrices M_{ij} and K_{ij} are well known from the finite-element literature to be symmetric positive definite (Brenner and Scott, 2002) and thus all the eigenvalues are real and positive (Watkins, 2002). The eigenvalues for the semidiscrete case, equation 7, have the form $\Lambda = \omega_h^2$, and for the finite-difference in time case, equation 9, the eigenvalues have the form $\Lambda = \frac{4}{\Delta t^2}\sin^2\frac{\omega_h \Delta t}{2}$, where ω_h is the angular frequency at which the wave travels in the grid. We will use this after solving the eigenvalue problem to derive the grid-dispersion relations. It should be noted that we use the term *grid-dispersion relation* to mean an equation to calculate the velocity with which the wave travels in the grid normalized with the true velocity (e.g., Alford et al., 1974; Mullen and Belytschko, 1982; Moczo et al., 2000a).

The size of the eigenvalue problem 23 depends on the total number of nodes. We will not attempt to solve for the eigenvalues of equation 23 to get the grid dispersion since that would be an intractable problem in an unbounded domain. Instead we will use the assumptions previously given to reduce the order of the problem. To obtain a reduced-order eigenvalue problem we first note that in a regular grid using tensor product elements with $\kappa + 1$ nodes per element in each direction we will have only κ^2 classes of degrees of freedom, as shown in Figure 1 (Marfurt, 1984; Cohen, 2002). Thus, we only need to get the corresponding κ^2 eigenvalues.

To derive an eigenvalue equation of order κ^2, let us write M_{ij} and K_{ij} as fourth-order tensors using the definitions of the mass and stiffness matrices (equation 8) and the definition of the basis functions (equation 21):

$$\begin{aligned} M_{ij} &= \int_\Omega \phi_i(x,z)\phi_j(x,z)\, dx\, dz \\ &= \int_\Omega \varphi_{m_1}(x)\varphi_{m_2}(z)\varphi_{n_1}(x)\varphi_{n_2}(z)\, dx\, dz \\ &= M_{m_1 m_2 n_1 n_2}, \end{aligned} \tag{24}$$

$$\begin{aligned} K_{ij} &= \alpha^2 \int_\Omega \nabla\phi_i \cdot \nabla\phi_j\, dx\, dz \\ &= \alpha^2 \int_\Omega \nabla(\varphi_{m_1}(x)\varphi_{m_2}(z)) \cdot \nabla(\varphi_{n_1}(x)\varphi_{n_2}(z))\, dx\, dz \\ &= K_{m_1 m_2 n_1 n_2}, \end{aligned} \tag{25}$$

with $i = (\kappa + 1)m_2 + m_1$ and $j = (\kappa + 1)n_2 + n_1$. We can also write P_j as a second-order tensor by changing the index to $j = (\kappa + 1)n_2 + n_1$ to get (no summation over n_1 and n_2)

$$P_j = P_{n_1 n_2} = A_{n_1 n_2} e^{i(k_x x_{n_1} + k_z z_{n_2} - \omega t)}. \tag{26}$$

Furthermore, since the nodes are κ-periodic in both directions, we have that the constants $A_{n_1 n_2}$ are also κ-periodic, and thus

$$A_{n_1 n_2} = A_{(\kappa q_1 + \ell_1)(\kappa q_2 + \ell_2)} = A_{\ell_1 \ell_2}, \tag{27}$$

with $n_1 = \kappa q_1 + \ell_1$, $n_2 = \kappa q_2 + \ell_2$, and $0 \le \ell_1, \ell_2 < \kappa$. Substituting equations 24, 26, and 27 in the left-hand side of equation 23 we get

$$\begin{aligned} M_{m_1 m_2 n_1 n_2} P_{n_1 n_2} &= M_{m_1 m_2 n_1 n_2} A_{n_1 n_2} e^{i(k_x x_{n_1} + k_z z_{n_2} - \omega t)} \\ &= M_{m_1 m_2 (\kappa q_1 + \ell_1)(\kappa q_2 + \ell_2)} \\ &\quad \times e^{i(k_x h q_1 + k_z h q_2)} A_{\ell_1 \ell_2} \\ &\quad \times e^{i(k_x h \xi_{\ell_1} + k_z h \xi_{\ell_2} - \omega t)} \\ &= \tilde{M}_{m_1 m_2 \ell_1 \ell_2}(k_x, k_z) \tilde{A}_{\ell_1 \ell_2}(k_x, k_z) e^{-i\omega t}, \end{aligned} \tag{28}$$

and similarly, substituting equations 25–27 on the right-hand side, we obtain

$$K_{m_1 m_2 n_1 n_2} P_{n_1 n_2} = \tilde{K}_{m_1 m_2 \ell_1 \ell_2}(k_x, k_z) \tilde{A}_{\ell_1 \ell_2}(k_x, k_z) e^{-i\omega t}, \tag{29}$$

where

$$\tilde{M}_{m_1 m_2 \ell_1 \ell_2}(k_x, k_z) = M_{m_1 m_2 (\kappa q_1 + \ell_1)(\kappa q_2 + \ell_2)} e^{i(k_x h q_1 + k_z h q_2)}, \tag{30}$$

$$\tilde{K}_{m_1 m_2 \ell_1 \ell_2}(k_x, k_z) = K_{m_1 m_2 (\kappa q_1 + \ell_1)(\kappa q_2 + \ell_2)} e^{i(k_x h q_1 + k_z h q_2)}, \tag{31}$$

and

$$\tilde{A}_{\ell_1 \ell_2}(k_x, k_z) = A_{\ell_1 \ell_2} e^{i(k_x h \xi_{\ell_1} + k_z h \xi_{\ell_2})}. \tag{32}$$

Note that a summation is implied over q_1 and q_2 (but not on ℓ_1 and ℓ_2), and that the summations are always finite, even in an unbounded domain, because the mass and stiffness matrices are sparse.

Substituting equations 28 and 29 in equation 23 and eliminating the $e^{-i\omega t}$ factor we get the following reduced-order eigenvalue equation (Appendix A):

$$\Lambda \tilde{M}_{m_1 m_2 \ell_1 \ell_2} \tilde{A}_{\ell_1 \ell_2} = \tilde{K}_{m_1 m_2 \ell_1 \ell_2} \tilde{A}_{\ell_1 \ell_2}, \quad 0 \le m_1, m_2 < \kappa. \tag{33}$$

The eigenvectors $\widetilde{A}_{\ell_1\ell_2}$, as defined in equation 32, are explicitly dependent on the node coordinates, but the eigenvalues depend on the grid nodes only in the sense that the nodes are used to compute the mass and stiffness matrices. In practice, this means that to obtain the grid dispersion, we will use only the node's coordinates to compute the integrals in equation 8 (thus avoiding the difficulty caused by irregular node spacing).

The above eigenvalue problem can be reduced to two eigenvalue problems of order κ each by making the following observation. Using the definition of the mass and stiffness matrices, for tensor-product rectangular elements and for a regular mesh we can write (see Appendix B):

$$M_{m_1m_2n_1n_2} = M^{1D}_{m_1n_1} M^{1D}_{m_2n_2} \tag{34}$$

and

$$K_{m_1m_2n_1n_2} = K^{1D}_{m_1n_1} M^{1D}_{m_2n_2} + K^{1D}_{m_2n_2} M^{1D}_{m_1n_1}, \tag{35}$$

where M^{1D}_{mn} and K^{1D}_{mn} are the mass and stiffness matrices of the 1D problem given by

$$M^{1D}_{mn} = \int_{x_0}^{x_1} \varphi_m \varphi_n dx \tag{36}$$

and

$$K^{1D}_{mn} = \alpha^2 \int_{x_0}^{x_1} \varphi'_m \varphi'_n dx. \tag{37}$$

We can use this result to further show that

$$\widetilde{M}_{m_1m_2n_1n_2}(k_x,k_z) = \widetilde{M}^{1D}_{m_1n_1}(k_x)\widetilde{M}^{1D}_{m_2n_2}(k_z) \tag{38}$$

and

$$\widetilde{K}_{m_1m_2n_1n_2}(k_x,k_z) = \widetilde{K}^{1D}_{m_1n_1}(k_x)\widetilde{M}^{1D}_{m_2n_2}(k_z) + \widetilde{K}^{1D}_{m_2n_2}(k_z)\widetilde{M}^{1D}_{m_1n_1}(k_x), \tag{39}$$

where (summation is implied over ℓ on the right-hand side)

$$\widetilde{M}^{1D}_{mn}(k_\eta) = M^{1D}_{m(\kappa\ell+n)} e^{ik_\eta h\ell} \tag{40}$$

and

$$\widetilde{K}^{1D}_{mn}(k_\eta) = K^{1D}_{m(\kappa\ell+n)} e^{ik_\eta h\ell} \tag{41}$$

(see Appendix B).

Substituting this decomposition of the mass and stiffness matrices into the eigenvalue problem we find that the eigenvalues can be expressed as a combination of the eigenvalues of the 1D problems. Let λ_1 be an eigenvalue of $\lambda_1 \widetilde{M}^{1D}_{ij}(k_x)\widetilde{A}_j = \widetilde{K}^{1D}_{ij}(k_x)\widetilde{A}_j$, and λ_2 be an eigenvalue of $\lambda_2 \widetilde{M}^{1D}_{ij}(k_z)\widetilde{A}_j = \widetilde{K}^{1D}_{ij}(k_z)\widetilde{A}_j$. Then the eigenvalues of $\Lambda \widetilde{M}_{ijkl}(k_x,k_z)\widetilde{A}_{kl} = \widetilde{K}_{ijkl}(k_x,k_z)\widetilde{A}_{kl}$ are given by $\Lambda = \lambda_1 + \lambda_2$ (see Appendix B).

As the degree of the polynomials gets higher it becomes impractical to derive an explicit grid-dispersion relation, but we can always obtain the κ eigenvalues numerically in each direction and use them to compute the grid dispersion. In seismic modeling there is only one eigenvalue with physical meaning; all the other eigenvalues correspond to nonphysical modes. In the 1D case it has been shown that the nonphysical modes have a negligible effect on the solution (Mulder, 1999; Cohen, 2002). It is reasonable to expect the same behavior on higher dimensions, but we are not aware of a proof, and it is beyond the scope of this paper. We have found through numerical experiments that the eigenvalue that corresponds to the acoustic wave is the smallest one. Further research is needed to ascertain the validity of this hypothesis.

To obtain the stability condition, we first consider the eigenvalues of equation 33 for the case $\alpha = 1$ and $h = 1$, where α is the acoustic wave velocity and h is the size of one side of the element. From the definition of the mass and stiffness matrices (equation 8), we have

$$\widetilde{M}_{m_1m_2\ell_1\ell_2} = h\widetilde{M}'_{m_1m_2\ell_1\ell_2} \quad \text{and} \quad \widetilde{K}_{m_1m_2\ell_1\ell_2} = \frac{\alpha^2}{h}\widetilde{K}'_{m_1m_2\ell_1\ell_2}, \tag{42}$$

where $\widetilde{M}'_{m_1m_2\ell_1\ell_2}$ and $\widetilde{K}'_{m_1m_2\ell_1\ell_2}$ are computed using $\alpha = 1$ and $h = 1$. Let Λ' be an eigenvalue of $\Lambda'\widetilde{M}'_{m_1m_2\ell_1\ell_2}\widetilde{A}_{\ell_1\ell_2} = \widetilde{K}'_{m_1m_2\ell_1\ell_2}\widetilde{A}_{\ell_1\ell_2}$. Using equations 42, we have that Λ' is related to the eigenvalue Λ of equation 33 by $\Lambda = \alpha^2\Lambda'/h^2$. Now, using the definition of the eigenvalues for the finite-difference in time case, $\Lambda = \frac{4}{\Delta t^2}\sin^2\frac{\omega_h \Delta t}{2}$, yields

$$\frac{q^2}{4}\Lambda' = \sin^2\frac{\omega_h \Delta t}{2} \le 1, \tag{43}$$

where $q = \alpha\Delta t/h$ is the stability parameter. Equivalently, the inequality 43 can be written as $q \le 2/\sqrt{\Lambda'}$. Note that Λ' is a function of the wavenumber through equations 28 and 29, and that the above inequality must be satisfied for all the eigenvalues and all the wavenumbers; thus, we write

$$q \le \min_{1\le j\le\kappa^2} \min_{0\le\theta\le 2\pi} 2\Lambda'_j(\theta)^{-1/2}, \tag{44}$$

where θ is the angle of incidence, defined as the angle between the wavenumber vector and the z-axis.

The grid-dispersion relations are given as follows. Let Λ be the smallest eigenvalue of equation 33 using $h = 1$ and $\alpha = 1$. Then from the definition of the eigenvalues in the semidiscrete case we have that $\omega_h = (\alpha/h)\sqrt{\Lambda}$. Substituting $\omega_h = 2\pi\alpha_h s/h$ and multiplying by $h/(2\pi\alpha s)$ we get

$$\frac{\alpha_h}{\alpha} = \frac{1}{2\pi s}\sqrt{\Lambda}, \tag{45}$$

where α_h is the velocity at which the wave travels in the grid, $s = h/(\kappa L)$ is the average sampling ratio in the element, and L is the wavelength. Similarly, for the finite-difference in time case, we obtain

$$\frac{\alpha_h}{\alpha} = \frac{1}{\pi s q}\sin^{-1}\left(\frac{q}{2}\sqrt{\Lambda}\right). \tag{46}$$

The procedure to derive the grid dispersion for a given order, sampling ratio, and wavenumber is summarized below:

1) Compute the 1D mass and stiffness matrices with equations 36 and 37 using $h = 1$ and $\alpha = 1$.
2) Compute $\widetilde{M}^{1D}_{mn}(k_x)$, $\widetilde{M}^{1D}_{mn}(k_z)$, $\widetilde{K}^{1D}_{mn}(k_x)$, and $\widetilde{K}^{1D}_{mn}(k_z)$ using equations 40 and 41.
3) Solve the eigenvalue problems $\lambda_1 \widetilde{M}^{1D}_{ij}(k_x)\widetilde{A}_j = \widetilde{K}^{1D}_{ij}(k_x)\widetilde{A}_j$, and

$\lambda_2\widetilde{M}^{1D}_{ij}(k_z)\widetilde{A}_j = \widetilde{K}^{1D}_{ij}(k_z)\widetilde{A}_j$, and save the smallest eigenvalue; recall that the eigenvalue of the 2D problem is $\Lambda = \lambda_1 + \lambda_2$.

4) Calculate the grid dispersion using equation 45 for the semidiscrete case or equation 46 for the finite-difference in time case.

Examples

Let us now derive explicitly the grid-dispersion relations for the lowest-order CFEM and SEM using finite differences in time. For first-order methods we will have one degree of freedom; thus we can easily solve for the eigenvalue. For CFEM, doing exact integration in equation 36 and substituting in equations 40 and 41, we get

$$\widetilde{M}^{1D}(k_\eta) = \frac{2 + \cos(k_\eta h)}{3} \tag{47}$$

and

$$\widetilde{K}^{1D}(k_\eta) = 2 - 2\cos(k_\eta h). \tag{48}$$

Therefore the eigenvalue of the 2D problem (step 3) is given by

$$\begin{aligned}\Lambda &= \frac{\widetilde{K}^{1D}(k_x)}{\widetilde{M}^{1D}(k_x)} + \frac{\widetilde{K}^{1D}(k_z)}{\widetilde{M}^{1D}(k_z)} \\ &= 6\frac{1 - 1\cos(k_x h)}{2 + \cos(k_x h)} + 6\frac{1 - 1\cos(k_z h)}{2 + \cos(k_z h)}.\end{aligned} \tag{49}$$

From this we have that the stability condition is given by $q \le 6^{-1/2}$, and the grid-dispersion relation is

$$\frac{\alpha_h}{\alpha} = \frac{1}{\pi s \mathrm{q}}\sin^{-1}\left(\mathrm{q}\sqrt{\frac{12 - 3\cos(k_x h) - 3\cos(k_z h) - 6\cos(k_x h)\cos(k_z h)}{8 + 4\cos(k_x h) + 4\cos(k_z h) + 2\cos(k_x h)\cos(k_z h)}}\right). \tag{50}$$

An equivalent equation for the semidiscrete case was given in Mullen and Belytschko (1982) using a different approach.

In the SEM case, we use the trapezoidal rule of integration in equation 36. Substituting the results in equations 40 and 41 and solving for the eigenvalue, we get

$$\Lambda = \frac{2\alpha^2}{h^2}\big(2 - \cos(k_x h) - \cos(k_z h)\big). \tag{51}$$

From this we have that the stability condition for this scheme is $q \le 2^{-1/2}$. If we substitute this eigenvalue in equation 46, we obtain the following grid-dispersion relation

$$\frac{\alpha_h}{\alpha} = \frac{1}{\pi s \mathrm{q}}\sin^{-1}\big(q\sqrt{\sin^2(\pi s\cos\theta) + \sin^2(\pi s\sin\theta)}\big), \tag{52}$$

which is the same as that for the acoustic FDM (Alford et al., 1974), as expected, because the first-order acoustic SEM is equivalent to the acoustic FDM (Cohen, 2002).

Elastic case

In this section we will show how to compute the grid dispersion of the elastic CFEM and SEM schemes. The approach is similar to the one used for the acoustic case and is based on a generalized eigenvalue problem which can be reduced to order $2\kappa^2$ by making some assumptions. One difference is that here we will not be able to reduce the eigenvalue problem to one of getting the eigenvalues of a 1D problem. Nevertheless, we can compute the $2\kappa^2$ eigenvalues numerically. A method to compute the grid dispersion and explicit grid-dispersion relations for first-order SEM will be given at the end of this section.

Again we make use of the von Neumann method (Mitchell and Griffiths, 1980; Hughes, 1987) and assume that all the elements in the domain are square with sides h. The nodes are defined the same way as in the acoustic case, but now we have two degrees of freedom at each one.

If we assume that the solution is a plane wave, then U^x_j and U^z_j have the form (no summation over j)

$$U^x_j(t) = A_j e^{i(\mathbf{k}\cdot\mathbf{x}_j - \omega t)} \tag{53}$$

and

$$U^z_j(t) = B_j e^{i(\mathbf{k}\cdot\mathbf{x}_j - \omega t)}. \tag{54}$$

Substituting in equations 12 and 13, or in equations 19 and 20, we get

$$\Lambda M_{ij}U^x_j = K^1_{ij}U^x_j + K^2_{ij}U^z_j \tag{55}$$

and

$$\Lambda M_{ij}U^z_j = K^3_{ij}U^x_j + K^4_{ij}U^z_j, \tag{56}$$

where M_{ij}, K^1_{ij}, K^2_{ij}, K^3_{ij}, and K^4_{ij} are given in equations 14 to 18, and the eigenvalues are given by $\Lambda = \omega_h^2$ for the semidiscrete case and $\Lambda = \frac{4}{\Delta t^2}\sin^2\frac{\omega_h\Delta t}{2}$ for the finite difference in time case. The above equations represent a generalized eigenvalue problem; this is clearly seen if we write

$$\Lambda\begin{bmatrix}\mathbf{M} & 0\\ 0 & \mathbf{M}\end{bmatrix}\begin{bmatrix}\mathbf{U}^x\\ \mathbf{U}^z\end{bmatrix} = \begin{bmatrix}\mathbf{K}^1 & \mathbf{K}^2\\ \mathbf{K}^3 & \mathbf{K}^4\end{bmatrix}\begin{bmatrix}\mathbf{U}^x\\ \mathbf{U}^z\end{bmatrix}, \tag{57}$$

where $(\mathbf{M})_{ij} = M_{ij}$, $(\mathbf{K}^l)_{ij} = K^\ell_{ij}$, $(\mathbf{U}^x)_j = U^x_j$, and $(\mathbf{U}^z)_j = U^z_j$. It can be shown that the eigenvalues of the above system are real and positive (see Appendix C).

Proceeding as we did for the acoustic case, we write these matrices as fourth-order tensors and as a combination of the corresponding matrices of the 1D problem

$$M_{ij} = M_{m_1m_2n_1n_2} = \frac{r^2}{\alpha^2}M^{1D}_{m_1n_1}M^{1D}_{m_2n_2}, \tag{58}$$

$$K^1_{ij} = K^1_{m_1m_2n_1n_2} = r^2K^{1D}_{m_1n_1}M^{1D}_{m_2n_2} + K^{1D}_{m_2n_2}M^{1D}_{m_1n_1}, \tag{59}$$

$$\begin{aligned}K^2_{ij} &= K^2_{m_1m_2n_1n_2} = (r^2 - 1)C^{1D}_{m_1n_1}C^{1D}_{n_2m_2} \\ &= (1 - r^2)C^{1D}_{m_1n_1}C^{1D}_{m_2n_2},\end{aligned} \tag{60}$$

$$K^3_{ij} = K^3_{m_1m_2n_1n_2} = K^2_{m_1m_2n_1n_2}, \tag{61}$$

and

$$K^4_{ij} = K^4_{m_1m_2n_1n_2} = K^{1D}_{m_1n_1}M^{1D}_{m_2n_2} + r^2K^{1D}_{m_2n_2}M^{1D}_{m_1n_1}, \tag{62}$$

where $i = (\kappa + 1)n_1 + m_1$, $j = (\kappa + 1)n_2 + m_2$, and

$$M^{1D}_{mn} = \int_{x_0}^{x_1} \varphi_m \varphi_n dx, \tag{63}$$

$$K^{1D}_{mn} = \int_{x_0}^{x_1} \varphi'_m \varphi'_n dx, \tag{64}$$

and

$$C^{1D}_{mn} = \int_{x_0}^{x_1} \varphi'_m \varphi_n dx. \tag{65}$$

Writing U^x_j and U^z_j with two indices using $j = (\kappa + 1)n_2 + n_1$ as well, we get

$$U^x_j = U^x_{n_1 n_2} = A_{n_1 n_2} e^{\mathrm{i}(k_x x_{n_1} + k_z z_{n_2} - \omega t)} \tag{66}$$

and

$$U^z_j = U^z_{n_1 n_2} = B_{n_1 n_2} e^{\mathrm{i}(k_x x_{n_1} + k_z z_{n_2} - \omega t)}. \tag{67}$$

Because the nodes are κ-periodic in each direction, we have $2\kappa^2$ degrees of freedom and, as in the acoustic case, the constants are also κ-periodic. Thus,

$$A_{n_1 n_2} = A_{(\kappa q_1 + \ell_1)(\kappa q_2 + \ell_2)} = A_{\ell_1 \ell_2} \tag{68}$$

and

$$B_{n_1 n_2} = B_{(\kappa q_1 + \ell_1)(\kappa q_2 + \ell_2)} = B_{\ell_1 \ell_2} \tag{69}$$

for $n_1 = \kappa q_1 + \ell_1$, $n_2 = \kappa q_2 + \ell_2$, and $0 \le \ell_1, \ell_2 < \kappa$. Substituting in equations 55 and 56 and eliminating the $e^{-\mathrm{i}\omega t}$ factor, we have the following eigenvalue problem of order $2\kappa^2$:

$$\Lambda \widetilde{M}_{m_1 m_2 n_1 n_2} \widetilde{A}_{n_1 n_2} = \widetilde{K}^1_{m_1 m_2 n_1 n_2} \widetilde{A}_{n_1 n_2} + \widetilde{K}^2_{m_1 m_2 n_1 n_2} \widetilde{B}_{n_1 n_2} \tag{70}$$

and

$$\Lambda \widetilde{M}_{m_1 m_2 n_1 n_2} \widetilde{B}_{n_1 n_2} = \widetilde{K}^2_{m_1 m_2 n_1 n_2} \widetilde{A}_{n_1 n_2} + \widetilde{K}^4_{m_1 m_2 n_1 n_2} \widetilde{B}_{n_1 n_2} \tag{71}$$

for $0 \le m_1, m_2, n_1, n_2 < \kappa$, where

$$\widetilde{M}_{m_1 m_2 n_1 n_2}(k_x, k_z) = \frac{r^2}{\alpha^2} \widetilde{M}^{1D}_{m_1 n_1}(k_x) \widetilde{M}^{1D}_{m_2 n_2}(k_z), \tag{72}$$

$$\widetilde{K}^1_{m_1 m_2 n_1 n_2}(k_x, k_z) = r^2 \widetilde{K}^{1D}_{m_1 n_1}(k_x) \widetilde{M}^{1D}_{m_2 n_2}(k_z) + \widetilde{K}^{1D}_{m_2 n_2}(k_z) \widetilde{M}^{1D}_{m_1 n_1}(k_x), \tag{73}$$

$$\widetilde{K}^2_{m_1 m_2 n_1 n_2}(k_x, k_z) = (1 - r^2) \widetilde{C}^{1D}_{m_1 n_1}(k_x) \widetilde{C}^{1D}_{m_2 n_2}(k_z), \tag{74}$$

$$\widetilde{K}^4_{m_1 m_2 n_1 n_2}(k_x, k_z) = \widetilde{K}^{1D}_{m_1 n_1}(k_x) \widetilde{M}^{1D}_{m_2 n_2}(k_z) + r^2 \widetilde{K}^{1D}_{m_2 n_2}(k_z) \widetilde{M}^{1D}_{m_1 n_1}(k_x), \tag{75}$$

$$\widetilde{A}_{n_1 n_2}(k_x, k_z) = A_{n_1 n_2} e^{\mathrm{i}(k_x \xi_{n_1} + k_z \xi_{n_2})}, \tag{76}$$

$$\widetilde{B}_{n_1 n_2}(k_x, k_z) = B_{n_1 n_2} e^{\mathrm{i}(k_x \xi_{n_1} + k_z \xi_{n_2})}, \tag{77}$$

$$\widetilde{M}^{1D}_{mn}(k_\eta) = M^{1D}_{m(\kappa\ell + n)} e^{\mathrm{i}k_\eta h\ell}, \tag{78}$$

$$\widetilde{K}^{1D}_{mn}(k_\eta) = K^{1D}_{m(\kappa\ell + n)} e^{\mathrm{i}k_\eta h\ell}, \tag{79}$$

and

$$\widetilde{C}^{1D}_{mn}(k_\eta) = C^{1D}_{m(\kappa\ell + n)} e^{\mathrm{i}k_\eta h\ell}. \tag{80}$$

In general, for higher-order polynomials we will have more eigenvalues than physical modes. If that is the case, we have found through numerical experimentation that the smallest eigenvalue corresponds to the S-wave dispersion, the next to the P-wave and the others to the nonphysical modes; further research is needed to prove this hypothesis. The stability condition is similar to the one for the acoustic scheme:

$$q \le \min_{1 \le j \le 2\kappa^2} \min_{0 \le \theta \le 2\pi} 2\Lambda_j(\theta)^{-1/2}, \tag{81}$$

where $\Lambda_j(\theta)$ are the eigenvalues of the system 70 and 71 using $h = 1$, $k_x h = \pi s \cos\theta$, and $k_z h = \pi s \sin\theta$ to compute $\widetilde{M}_{m_1 m_2 \ell_1 \ell_2}$, $\widetilde{K}^1_{m_1 m_2 \ell_1 \ell_2}$, $\widetilde{K}^2_{m_1 m_2 \ell_1 \ell_2}$, and $\widetilde{K}^4_{m_1 m_2 \ell_1 \ell_2}$ (see the explanation leading to equation 44).

The procedure to derive the grid dispersion for a given order, sampling ratio, and wavenumber is described below.

1) Compute the 1D mass and stiffness matrices with equations 63 to 65 using $h = 1$.
2) Compute $\widetilde{M}^{1D}_{mn}(k_x)$, $\widetilde{M}^{1D}_{mn}(k_z)$, $\widetilde{K}^{1D}_{mn}(k_x)$, $\widetilde{K}^{1D}_{mn}(k_z)$, $\widetilde{C}^{1D}_{mn}(k_x)$, and $\widetilde{C}^{1D}_{mn}(k_z)$ using equations 78 to 80.
3) Build the block matrices of the eigenvalue problem using equations 72 to 75 with $\alpha = 1$.
4) Solve the eigenvalue problem of equations 70 and 71 and save the two smallest eigenvalues. Call these Λ_1 and Λ_2, respectively.
5) Calculate the grid dispersion using, for the semidiscrete case,

$$\frac{\alpha_h}{\alpha} = \frac{1}{2\pi s} \sqrt{\Lambda_2} \tag{82}$$

and

$$\frac{\beta_h}{\beta} = \frac{r}{2\pi s} \sqrt{\Lambda_1}, \tag{83}$$

and for the finite differences in time case,

$$\frac{\alpha_h}{\alpha} = \frac{1}{\pi s q} \sin^{-1}\left(\frac{\mathrm{q}}{2}\sqrt{\Lambda_2}\right) \tag{84}$$

and

$$\frac{\beta_h}{\beta} = \frac{r}{\pi s q} \sin^{-1}\left(\frac{\mathrm{q}}{2}\sqrt{\Lambda_1}\right). \tag{85}$$

Example

Let us consider, the first-order SEM. For this case, we have two degrees of freedom, and we can solve the eigenvalue problem algebraically. Calculating the mass and stiffness matrices using the trapezoidal quadrature rule and substituting in equations 72 to 75, we obtain

$$\widetilde{\mathbf{M}}(k_x,k_z) = \frac{h^2 r^2}{\alpha^2}, \tag{86}$$

$$\widetilde{\mathbf{K}}^1(k_x,k_z) = 2r^2(1 - \cos(k_x h)) + 2(1 - \cos(k_z h)), \tag{87}$$

$$\widetilde{\mathbf{K}}^2(k_x,k_z) = (r^2 - 1)\sin(k_x h)\sin(k_z h), \tag{88}$$

and

$$\widetilde{\mathbf{K}}^4(k_x,k_z) = 2(1 - \cos(k_x h)) + 2r^2(1 - \cos(k_z h)). \tag{89}$$

Substituting these in equations 70 and 71, and solving the eigenvalue problem, we get $\Lambda_1 = \alpha^2(\gamma - \delta)/h^2$ and $\Lambda_2 = \alpha^2(\gamma + \delta)/h^2$, where

$$\gamma = (r^2 + 1)(2 - \cos(k_x h) - \cos(k_z h)) \tag{90}$$

and

$$\delta = (r^2 - 1) \times \sqrt{(\cos(k_x h) - \cos(k_z h))^2 + \sin^2(k_x h)\sin^2(k_z h)}. \tag{91}$$

Using equations 84 and 85 we obtain the following grid-dispersion relations:

$$\frac{\alpha_h}{\alpha} = \frac{1}{\pi s q}\sin^{-1}\left(\frac{q}{2}\sqrt{\gamma + \delta}\right) \tag{92}$$

and

$$\frac{\beta_h}{\beta} = \frac{r}{\pi s q}\sin^{-1}\left(\frac{q}{2}\sqrt{\gamma - \delta}\right). \tag{93}$$

The stability condition for this scheme is $q\sqrt{1 + 1/r^2} \le 1$. As expected, the stability condition and grid-dispersion relations are the same as those for the elastic standard grid FDM because the first-order elastic SEM is equivalent to the elastic standard grid FDM (Cohen, 2002).

RESULTS

In this section, we will present the grid-dispersion curves for the acoustic and elastic CFEM and SEM using the method that we presented in the previous section. We will describe the effect that the stability parameter (q, equation 43), the incidence angle (θ, equation 44), the sampling ratio (s, equation 45), the order of the elements (κ, see the "Basis Functions" subsection), and the P- to S-wave velocity ratio (r, equation 18, elastic case) have in the grid dispersion.

Acoustic schemes

In Figure 2, we plotted the grid-dispersion curves of the first-order SEM (equation 52) using q = 0.1 and q = 0.7. As we have noted before, this scheme is equivalent to the acoustic FDM, therefore we arrive at the same conclusions as those reported in Alford et al. (1974):

- The dispersion is greatest in the direction of any of the grid axes.
- The dispersion is smallest if we take a time step close to the stability condition,
- A minimum of 10 nodes per wave length ($s = 0.1$) is recommended to achieve accurate results.

It is clearly advantageous to use higher-order SEM, as concluded in Seriani and Priolo (1994), because not only does the dispersion diminish rapidly but also the anisotropy practically disappears in third- and higher-order SEMs (it is already small in second-order SEM; see Figures 3a and b).

Perhaps the most important advantage of using higher-order SEMS is that we can decrease the sampling ratio to four to five nodes per wave length (Seriani and Priolo, 1994). Comparing Figures 2b, 3a, and b, we note that in contrast to first-order SEMs, using second-order and above, we would introduce nonphysical arrivals because the grid velocity is slightly increased with respect to the physical velocity. Nevertheless, this increase in velocity is less than 1% for a sampling ratio of four to five nodes per wavelength.

Comparing CFEM, we observe approximately the same level of dispersion and anisotropy using second-order CFEM (Figure 4b) and second-order SEM (Figure 3a). Thus there is no loss of accuracy due to mass lumping. First-order CFEM (Figure 4a) suffers from the same anisotropy and dispersion as first-order SEM (Figure 2b), with the difference that the waves are hastened instead of delayed, as noted in Mullen and Belytschko (1982). In both first-order schemes we would need at least 10 nodes per wavelength to obtain accurate results.

To show the effect of a smaller time step in the higher-order SEM, we have plotted in Figure 5 the dispersion curves for $3 \le \kappa \le 10$ and for different values of q. We observe that if we take 4.5 nodes per wavelength, as suggested by Seriani and Priolo (1994), the dispersion is less than 1%, even at $q = 1$.

To illustrate the dispersive behavior of the acoustic SEM, in Figure 6, we show snapshots of acoustic wave propagation using elements of different order but a constant sampling ratio. The physical model is a homogeneous rectangle of 1 by 1 km with $\rho = 4$ kg/cm^3 and $\lambda = 1.8 \times 10^{10}$ Pa; the source is located at the center and has a peak frequency of 30 Hz. All the snapshots are taken at $t = 0.2$ s, and the number of nodes is kept constant at 4225. Note that, for a fixed sampling ratio, increasing the order of the elements reduces the grid dispersion and produces a less anisotropic result.

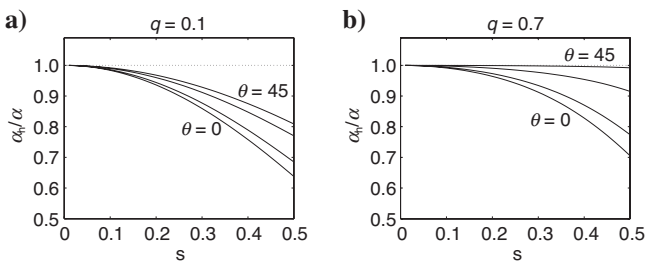

Figure 2. Grid dispersion of the acoustic FDM and first-order SEM as a function of the sampling ratio (s), equation 52, with incidence angles of $\theta = 0°$, 15°, 30°, and 45° and (a) $q = 0.1$ and (b) $q = 0.7$. The dispersion is minimized for an oblique incidence angle and for a time step close to the stability condition.

Elastic schemes

In the elastic schemes, the grid dispersion is dominated by the S-wave dispersion in an unbounded domain, and thus the sampling ratio is determined by the S-wave velocity. (In practice the domain usually is bounded, and thus the grid dispersion is dominated by the surface wave velocity). In Figures 7 through 12, we used the same sampling ratio for the P- and S-wave and we plotted the results for different ratios of P- to S-wave velocities.

In Figure 7, we have plotted equations 92 and 93 for different values of r and incidence angles. This is the grid dispersion of the standard grid FDM and of the first-order SEM, which are equivalent.

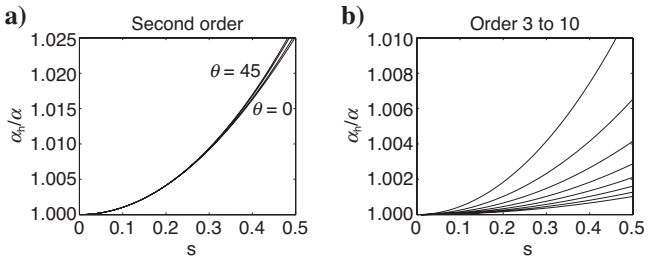

Figure 3. Grid dispersion of the SEM acoustic scheme for second-order and above, with $\theta = 0°, \ldots, 45°$ and $q = 0.5$. (a) Second-order SEM (9-node elements, $\kappa = 2$). (b) Third- to tenth-order SEM. The upper curve corresponds to $\kappa = 3$ and increases until $\kappa = 10$ for the lower one. Note the small anisotropy of the second-order scheme. For third order and above, the dispersion curves for different incidence angles are plotted on top of each other because they have negligible anisotropy.

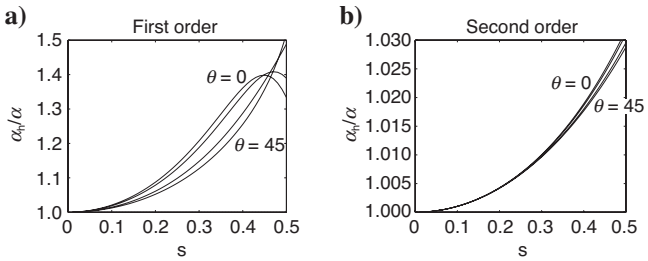

Figure 4. Grid dispersion of the CFEM acoustic scheme for $\theta = 0°, \ldots, 45°$ and $q = 0.5$. (a) First-order CFEM (four-node elements, equation 50). (b) Second-order CFEM (9-node elements). The first-order scheme has large and anisotropic dispersion. The second-order CFEM scheme has a dispersion similar to the dispersion of the second-order SEM (Figure 3a), with the difference that for an oblique incidence angle, the dispersion is the smallest.

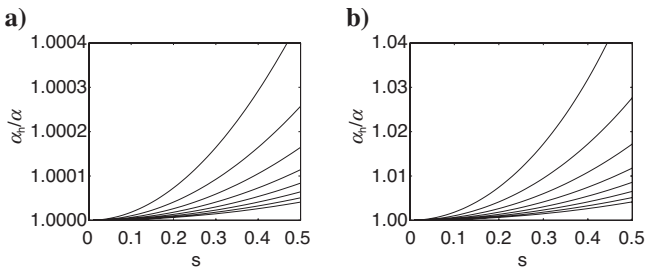

Figure 5. Grid dispersion as a function of the order of the SEM, with $\theta = 0°$, (a) $q = 0.1$, and, (b) $q = 1$. The upper curve corresponds to $\kappa = 3$, increasing up to $\kappa = 10$ for the lower curve. Note that the dispersion is proportional to the time step and inversely proportional to the order of the elements.

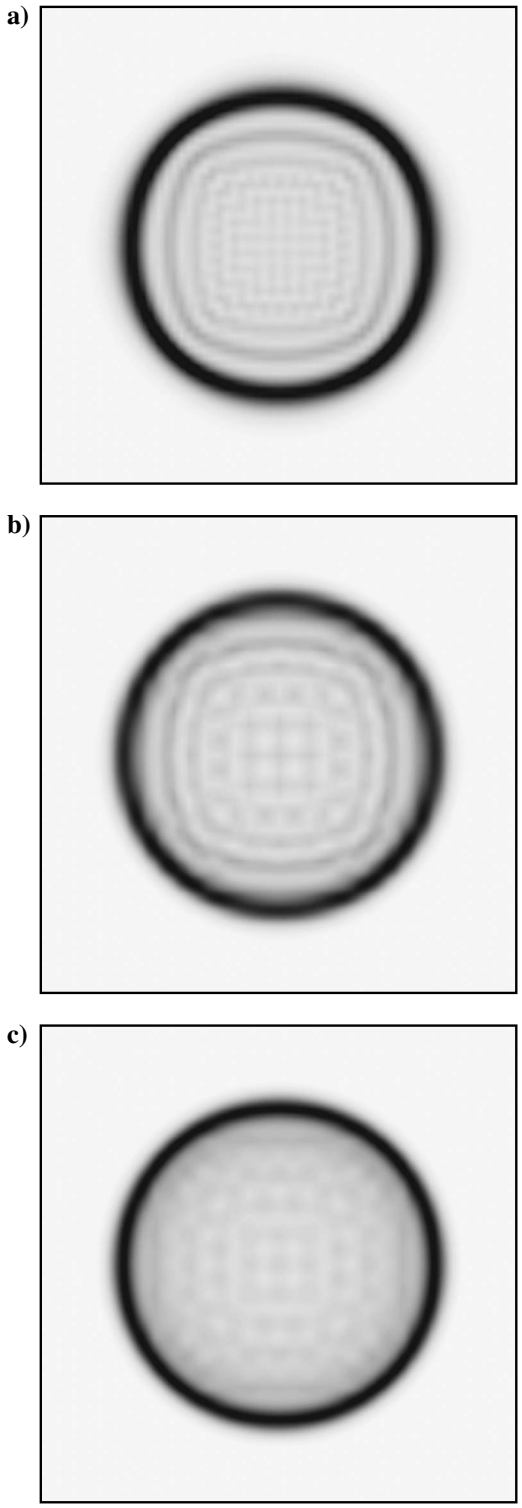

Figure 6. Snapshots at $t = 0.2$ of acoustic wave propagation using SEM. The model is a homogeneous rectangle of 1 by 1 km with $\rho = 4$ kg/cm^3 and $\lambda = 1.8 \times 10^{10}$ Pa; the source is located at the center and has a peak frequency of 30 Hz. (a) 4096 elements, $\kappa = 1$; (b) 1024 elements, $\kappa = 2$; (c) 256 elements, $\kappa = 4$. For comparison purposes, the number of nodes is 4225 in all the snapshots to keep a constant sampling ratio. Note that for a fixed sampling ratio, using higher-order polynomials reduces the dispersion.

From these figures we can see that the grid dispersion of the S-wave increases for increasing values of r. In particular, we note that for $r = 10$ (Poisson's ratio equal to 0.495) the S-wave travels at nearly twice the physical velocity using 10 nodes per wavelength. In practice this means that if we have a physical model with a liquid-solid interface we need to use a very high sampling ratio to obtain accurate results.

This disadvantage is overcome by the staggered-grid scheme. The grid dispersion of this scheme has been plotted in Figure 8 for different values of r and incidence angles. Note in these figures that the S-wave dispersion is nearly insensitive to r, and that the P-wave dispersion is negligible for the higher values of r. Therefore this scheme can be efficiently applied to models with liquid-solid interfaces.

In Figure 9, we have used first-order CFEM and we note that, although there is less dispersion than in the first-order SEM (Figure 7),

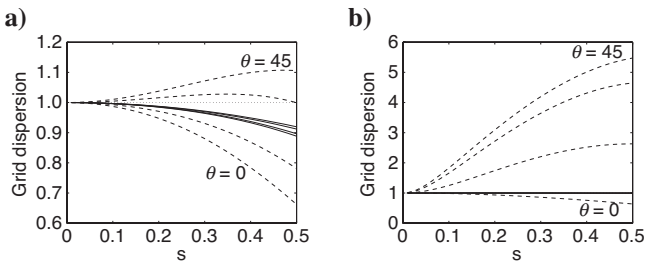

Figure 7. Grid dispersion in the elastic standard-grid FDM and first-order SEM as a function of the sampling ratio (equations 92 and 93) with $\theta = 0, \ldots, 45°$, $q = 0.7$ and (a) $r = 1.5$ and (b) $r = 10$. Solid lines correspond to the P-wave dispersion and dashed lines to the S-wave dispersion. The S-wave dispersion increases proportionally to r, introducing large anisotropic errors.

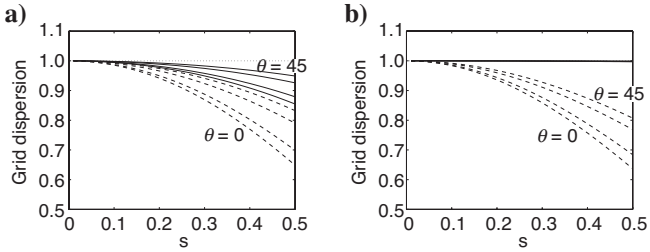

Figure 8. Grid dispersion in the staggered-grid FDM scheme using second-order differential operators with $\theta = 0, \ldots, 45°$, $q = 0.7$, and (a) $r = 1.5$, and (b) $r = 10$. Solid lines correspond to the P-wave dispersion and dashed lines to the S-wave dispersion. Note that the S-wave dispersion is not sensitive to r.

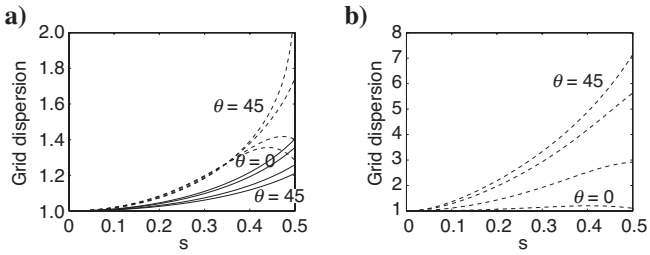

Figure 9. Grid dispersion for first-order elastic CFEM, with $\theta = 0, \ldots, 45°$, $q = 0.7$, and (a) $r = 1.5$, and (b) $r = 10$. Solid lines correspond to the P-wave dispersion and dashed lines to the S-wave dispersion. Like the first-order SEM (Figure 7), the S-wave dispersion increases proportionally to r and is strongly anisotropic.

it is not as accurate as the staggered-grid scheme. Comparing Figures 9a and b we observe that the grid dispersion and anisotropy increase with increasing values of r.

As noted for the acoustic case, it is also true for the elastic SEM that it is advantageous to use higher-order methods. In Figure 10, we can see that if we use a sampling ratio of 10 nodes per wavelength and second-order SEM, we get negligible dispersion and anisotropy even for large values of r. If we use higher-order SEM the dispersion diminishes very fast and the anisotropy disappears, and thus a lower sampling ratio is appropriate (see Figure 11). Comparing Figures 3b and 11b, we conclude that, as intuitively anticipated in Komatitsch et al. (2005), the dispersion results for the acoustic case indeed hold equally well for the elastic case because, for an order greater than three, the dispersion of the elastic scheme is smaller than the dispersion of the acoustic scheme.

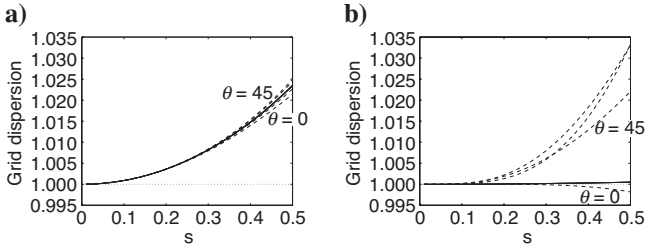

Figure 10. Grid dispersion for the second-order SEM, with $\theta = 0, \ldots, 45°$, $q = 0.7$, (a) $r = 1.5$, and (b) $r = 10$. Solid lines correspond to the P-wave dispersion and dashed lines to the S-wave dispersion. Note that if we use 10 nodes per wavelength ($s = 0.1$), we get negligible dispersion and anisotropy.

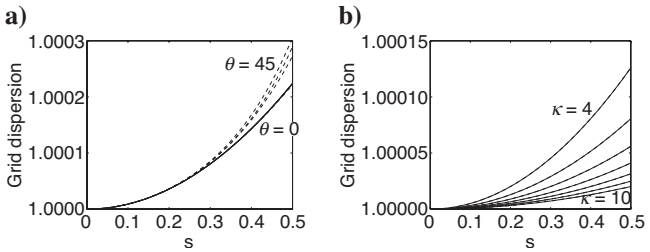

Figure 11. Grid dispersion as a function of the order of the SEM elastic schemes with $\theta = 0, \ldots, 45°$, $q = 0.7$, and $r = 10$. (a) Third-order SEM. Solid lines correspond to the P-wave dispersion and dashed lines to the S-wave. (b) Fourth- to tenth-order SEM. The upper curve corresponds to $\kappa = 4$ and increases up to $\kappa = 10$. The dispersion curves for different incidence angles are plotted on top of each other, showing that the dispersion is not angle dependent for fourth-order elements and above.

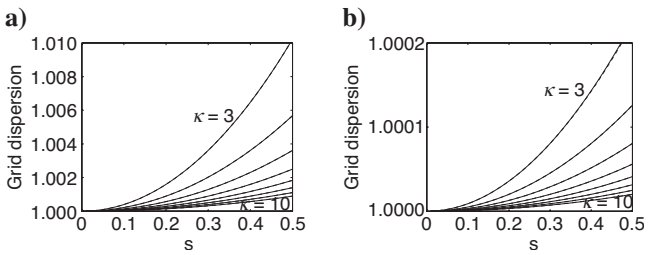

Figure 12. Grid dispersion as a function of the order of the SEM, with $\theta = 0°$, $q = 0.7$, (a) $r = 1.5$, and (b) $r = 10$. The upper curve corresponds to $\kappa = 3$, increasing up to $\kappa = 10$ for the lower curve. P- and S-wave dispersion curves overlap in these figures. Note that isotropy is preserved even for large values of r.

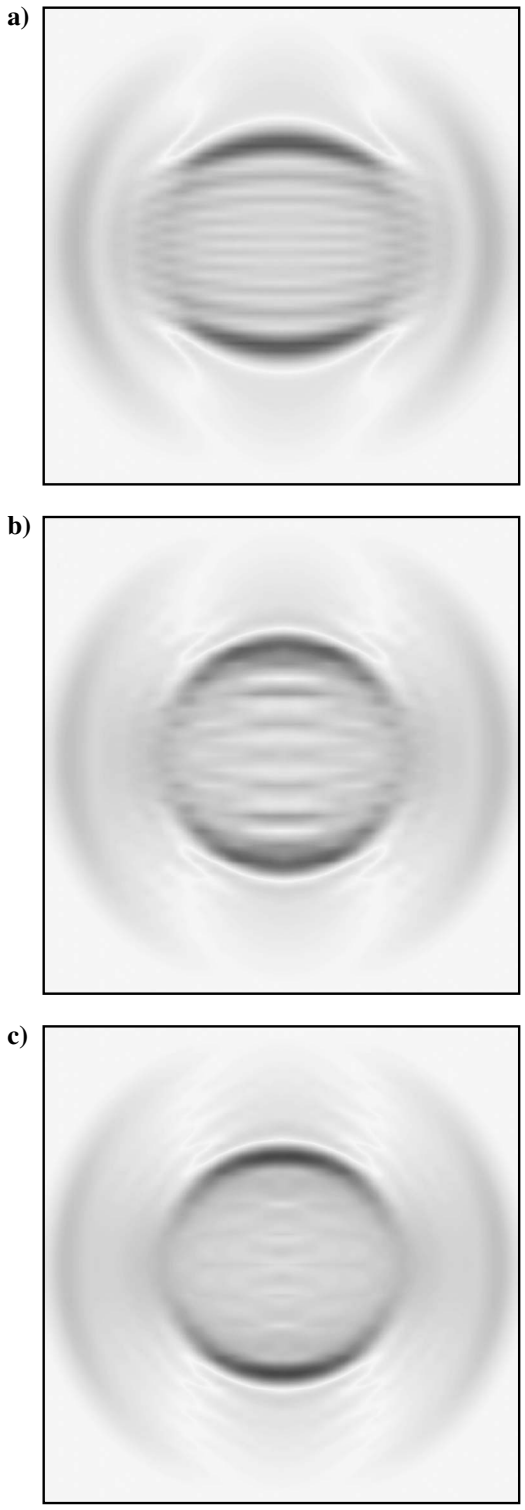

Figure 13. Snapshots at $t = 0.2$ of elastic wave propagation using SEM. The model is a homogeneous rectangle of 1 by 1 km with $\rho = 4$ kg/cm^3, $\lambda = 1.8 \times 10^{10}$ Pa, and $\mu = 9 \times 10^9$ Pa. The source is located at the center and has a peak frequency of 30 Hz. (a) 4096 elements, $\kappa = 1$; (b) 1024 elements, $\kappa = 2$; (c) 256 elements, $\kappa = 4$. For comparison purposes, the number of nodes is fixed at 4225 in all the snapshots, to keep a constant sampling ratio. Note that for a fixed sampling ratio, the use of higher-order polynomials reduces the dispersion.

To show the effect that the ratio of P- to S-wave velocity has on the higher-order SEM, we have plotted in Figure 12 the dispersion curves for $3 \leq \kappa \leq 10$ and for different values of r (compare to Figure 5, which is the limit for r tending to one). We observe that the isotropy is preserved and that the dispersion is less than 0.3% for 4.5 nodes per wavelength.

To illustrate the dispersive behavior of the elastic SEM, in Figure 13, we show snapshots of elastic wave propagation using elements of different order but keeping a constant sampling ratio. The physical model has the same characteristics as those of the acoustic model but with a shear modulus of $\mu = 9 \times 10^9$ Pa. All the snapshots are taken at $t = 0.2$ s, and the number of nodes is 4225. Note that, for a constant sampling ratio, increasing the order of the elements makes an improvement in the isotropy and reduces the dispersion.

CONCLUSIONS

We have derived stability conditions and analyzed the dispersive properties of the most common FEM methods. We presented a general approach to analyze acoustic and elastic FEM methods that overcomes the difficulties of analyzing SEM. Our approach includes previous results of FEM for quadrilateral tensor-product elements and FDM for the standard grid as special cases. Furthermore, this approach can be used to analyze the grid dispersion due only to the spatial discretization or the total grid dispersion, including the effects of the time stepping. We make the following remarks based on our analysis:

- SEM has approximately the same grid dispersion as CFEM. Thus, the mass lumping technique used in SEM achieves the goal of increasing performance while maintaining accuracy.
- Comparing first-order elastic CFEM and SEM we note that they both introduce anisotropic errors and are very sensitive to Poisson's ratio. CFEM also has the disadvantage of being an implicit scheme, and therefore it is inefficient for long propagation times.
- The SEM method of order four or greater is an accurate and efficient method for propagating acoustic and elastic waves. This method has the qualities of being isotropic and of introducing little dispersion in the results, making it adequate for simulations of long propagation times. Because of its low dispersion, the sampling ratio can be reduced to 4-5 nodes per wavelength with a negligible loss of accuracy.
- A comparison of the high-order SEM with the staggered-grid FDM reveals that they are both explicit and suitable for models with liquid-solid interfaces. SEM has the advantages of requiring a lower sampling ratio, having a smaller dispersion, and being isotropic. Furthermore, SEM has the flexibility to allow us to choose the order of the elements and adapt the elements to the medium discontinuities and surface topography.

We have restricted our analysis to the 2D case for tensor-product rectangular elements. We are currently working on the extension of this approach to the 3D case for tensor-product cubic elements and expect to extend the conclusions presented here to the 3D case as well. Other restrictions of our analysis are that we do not provide analytic solutions for arbitrary-order elements and we have considered only the second-order finite-difference scheme for time stepping.

Finally, we note that the grid-dispersion results presented here are the minimum dispersion for each of the methods. In practical applications more dispersion may arise from boundary conditions, irregular elements, or heterogeneities in the medium.

ACKNOWLEDGMENTS

The authors are grateful to Dimitri Komatitsch and Joe Dellinger for their careful review and valuable comments. This work was partially supported by the Airforce Research Laboratory, contract number FA8718-04-C-8014. This work was done while Jonas De Basabe was supported by a Ph.D. fellowship from the Mexican National Council for Science and Technology (CONACYT).

APPENDIX A

THE GRID DISPERSION RELATION AS A GENERALIZED EIGENVALUE PROBLEM

In this appendix, we explain the relation of equation 33 to a standard eigenvalue problem. We first note that the second-order tensor $\widetilde{A}_{\ell_1\ell_2}$ can be written as the vector

$$(\mathbf{V})_i = \widetilde{A}_{\ell_1\ell_2} \quad \forall\, i = \ell_2\kappa + \ell_1,\ 0 \le \ell_1,\ell_2 < \kappa. \tag{A-1}$$

Similarly, the fourth-order tensors $\widetilde{M}_{m_1m_2\ell_1\ell_2}$ and $\widetilde{K}_{m_1m_2\ell_1\ell_2}$ can be written as the matrices

$$(\mathbf{D})_{ji} = \widetilde{M}_{m_1m_2\ell_1\ell_2} \,\forall\, i = \ell_2\kappa + \ell_1,\ j = m_2\kappa + m_1,\quad 0 \le \ell_1,\ell_2,m_1,m_2 < \kappa \tag{A-2}$$

and

$$(\mathbf{E})_{ji} = \widetilde{K}_{m_1m_2\ell_1\ell_2} \,\forall\, i = \ell_2\kappa + \ell_1,\ j = m_2\kappa + m_1,\quad 0 \le \ell_1,\ell_2,m_1,m_2 < \kappa. \tag{A-3}$$

This can be written as a generalized eigenvalue problem:

$$\Lambda\mathbf{D}\mathbf{V} = \mathbf{E}\mathbf{V}. \tag{A-4}$$

Note that $\mathbf{V}$ has κ^2 elements and $\mathbf{D}$ and $\mathbf{E}$ have $\kappa^2 \times \kappa^2$ elements. If the inverse of $\mathbf{D}$ exists, this can be solved as the standard eigenvalue problem (Watkins, 2002)

$$\Lambda\mathbf{V} = (\mathbf{D}^{-1}\mathbf{E})\mathbf{V}. \tag{A-5}$$

For SEM, it can be shown that the mass matrix is diagonal (Komatitsch and Tromp, 1999; Cohen, 2002) therefore $\mathbf{D}$ can be trivially inverted, and the generalized eigenvalue problem can be solved as a standard eigenvalue problem. This is the approach used in Cohen (2002).

APPENDIX B

DECOMPOSITION OF THE EIGENVALUES

We will show in this appendix that the eigenvalues of equation 33 can be computed by the addition of the eigenvalues of the 1D problem. This proof is an extension of the proof in Cohen (2002), where a diagonal mass matrix is assumed. We show here that the results hold for a general mass matrix.

Let us first show how the 2D mass matrix can be decomposed into the corresponding 1D matrices (equation 34). Starting from the definition of the mass matrix, equation 24, we have

$$\begin{aligned} M_{m_1m_2n_1n_2} &= \int_\Omega \varphi_{m_1}(x)\varphi_{m_2}(z)\varphi_{n_1}(x)\varphi_{n_2}(z)\,dx\,dz \\ &= \int_\Omega \varphi_{m_1}(x)\varphi_{n_1}(x)\,dx \int_\Omega \varphi_{m_2}(z)\varphi_{n_2}(z)\,dz \\ &= M^{1D}_{m_1n_1} M^{1D}_{m_2n_2}. \end{aligned} \tag{B-1}$$

Similarly we can show the decomposition of the stiffness matrix (equation 35). From the definition of the stiffness matrix, equation 25, we have that

$$\begin{aligned} K_{m_1m_2n_1n_2} &= \alpha^2 \int_\Omega \nabla(\varphi_{m_1}(x)\varphi_{m_2}(z)) \\ &\quad \cdot \nabla(\varphi_{n_1}(x)\varphi_{n_2}(z))\,dx\,dz \\ &= \alpha^2 \int_\Omega (\varphi'_{m_1}(x)\varphi'_{n_1}(x)\varphi_{m_2}(z)\varphi_{n_2}(z) \\ &\quad + \varphi_{m_1}(x)\varphi_{n_1}(x)\varphi'_{m_2}(z)\varphi'_{n_2}(z))\,dx\,dz \\ &= \alpha^2 \int_\Omega \varphi'_{m_1}(x)\varphi'_{n_1}(x)\,dx \int_\Omega \varphi_{m_2}(z)\varphi_{n_2}(z)\,dz \\ &\quad + \alpha^2 \int_\Omega \varphi_{m_1}(x)\varphi_{n_1}(x)\,dx \int_\Omega \varphi'_{m_2}(z)\varphi'_{n_2}(z)\,dz \\ &= K^{1D}_{m_1n_1} M^{1D}_{m_2n_2} + K^{1D}_{m_2n_2} M^{1D}_{m_1n_1}. \end{aligned} \tag{B-2}$$

From these decompositions of the mass and stiffness matrices, we will demonstrate equations 38 and 39. Substituting the mass matrix decomposition in equation 30, we have that

$$\begin{aligned} \widetilde{M}_{m_1m_2\ell_1\ell_2}(k_x,k_z) &= M^{1D}_{m_1(\kappa q_1+\ell_1)} e^{ik_x hq_1} M^{1D}_{m_2(\kappa q_2+\ell_2)} e^{ik_z hq_2} \\ &= \widetilde{M}^{1D}_{m_1\ell_1}(k_x)\widetilde{M}^{1D}_{m_2\ell_2}(k_z). \end{aligned} \tag{B-3}$$

Substituting the stiffness-matrix decomposition in equation 31, we have that

$$\begin{aligned} \widetilde{K}_{m_1m_2\ell_1\ell_2}(k_x,k_z) &= (K^{1D}_{m_1(\kappa q_1+\ell_1)} M^{1D}_{m_2(\kappa q_2+\ell_2)} \\ &\quad + K^{1D}_{m_2(\kappa q_2+\ell_2)} M^{1D}_{m_1(\kappa q_1+\ell_1)}) e^{\mathrm{i}(k_x hq_1 + k_z hq_2)} \\ &= K^{1D}_{m_1(\kappa q_1+\ell_1)} e^{\mathrm{i}k_x hq_1} M^{1D}_{m_2(\kappa q_2+\ell_2)} e^{\mathrm{i}k_z hq_2} \\ &\quad + K^{1D}_{m_2(\kappa q_2+\ell_2)} e^{\mathrm{i}k_z hq_2} M^{1D}_{m_1(\kappa q_1+\ell_1)} e^{\mathrm{i}k_x hq_1} \\ &= \widetilde{K}^{1D}_{m_1\ell_1}(k_x)\widetilde{M}^{1D}_{m_2\ell_2}(k_z) \\ &\quad + \widetilde{K}^{1D}_{m_2\ell_2}(k_z)\widetilde{M}^{1D}_{m_1\ell_1}(k_x). \end{aligned} \tag{B-4}$$

Let λ_1 and $A^{(1)}_k$ satisfy

$$\lambda_1 \widetilde{M}^{1D}_{ik}(k_x) A^{(1)}_k = \widetilde{K}^{1D}_{ik}(k_x) A^{(1)}_k, \tag{B-5}$$

and let λ_2 and $A^{(2)}_j$ satisfy

$$\lambda_2 \widetilde{M}^{1D}_{jl}(k_z) A^{(2)}_l = \widetilde{K}^{1D}_{jl}(k_z) A^{(2)}_l. \quad \text{(B-6)}$$

Substituting the second-order tensor $B_{kl} = A^{(1)}_k A^{(2)}_l$ and the decomposition of the stiffness matrix in the right-hand side of equation 33, we have that

$$\begin{aligned}\widetilde{K}_{ijkl} B_{kl} &= (\widetilde{K}^{1D}_{ik}(k_x)\widetilde{M}^{1D}_{jl}(k_z) + \widetilde{K}^{1D}_{jl}(k_z)\widetilde{M}^{1D}_{ik}(k_x)) A^{(1)}_k A^{(2)}_l \\ &= \lambda_1 \widetilde{M}^{1D}_{ik}(k_x)\widetilde{M}^{1D}_{jl}(k_z) A^{(1)}_k A^{(2)}_l \\ &\quad + \lambda_2 \widetilde{M}^{1D}_{jl}(k_z)\widetilde{M}^{1D}_{ik}(k_x) A^{(1)}_k A^{(2)}_l \\ &= (\lambda_1 + \lambda_2)\widetilde{M}^{1D}_{ik}(k_x)\widetilde{M}^{1D}_{jl}(k_z) A^{(1)}_k A^{(2)}_l \\ &= (\lambda_1 + \lambda_2)\widetilde{M}_{ijkl} B_{kl}. \end{aligned} \quad \text{(B-7)}$$

Therefore, $\Lambda = \lambda_1 + \lambda_2$ is an eigenvalue of equation 33, with corresponding eigenvector B_{kl}. It can be easily shown by contradiction that all the eigenvalues of equation 33 can be expressed as a combination of the eigenvalues of the 1D problems by noting that all the possible combinations are κ^2, exactly the number of eigenvalues of equation 33.

APPENDIX C

ABOUT THE EIGENVALUES OF EQUATION 57

In this appendix, we will show that the eigenvalues of equation 57 are real and positive. It is sufficient to show that the matrices on the right- and left-hand sides are symmetric positive definite (Watkins, 2002). Let us first consider the matrix on the left-hand side. Multiplying the matrix by an arbitrary vector from the left and right yields

$$\begin{aligned}\begin{bmatrix}\mathbf{v}^T, & \mathbf{w}^T\end{bmatrix}\begin{bmatrix}\mathbf{M} & 0 \\ 0 & \mathbf{M}\end{bmatrix}\begin{bmatrix}\mathbf{v} \\ \mathbf{w}\end{bmatrix} &= \mathbf{v}^T\mathbf{M}\mathbf{v} + \mathbf{w}^T\mathbf{M}\mathbf{w} \\ &= M_{ij} v_i v_j + M_{ij} w_i w_j, \end{aligned} \quad \text{(C-1)}$$

where we have changed to index notation for convenience in the last step. In the first term, using the definition of M_{ij} given in equation 14, we get

$$M_{ij} v_i v_j = \int_\Omega \phi_i \phi_j v_i v_j \, dx \, dz = \int_\Omega (\phi_i v_i)^2 dx dz \geq 0 \quad \text{(C-2)}$$

and the same for the second term, thus the matrix on the left-hand side is symmetric positive definite. Let us now consider the matrix on the right-hand side. Multiplying the matrix by an arbitrary vector from the left and right yields

$$\begin{aligned}\begin{bmatrix}\mathbf{v}^T, & \mathbf{w}^T\end{bmatrix}\begin{bmatrix}\mathbf{K}^1 & \mathbf{K}^2 \\ \mathbf{K}^3 & \mathbf{K}^4\end{bmatrix}\begin{bmatrix}\mathbf{v} \\ \mathbf{w}\end{bmatrix} &= \mathbf{v}^T\mathbf{K}^1\mathbf{v} + \mathbf{v}^T\mathbf{K}^2\mathbf{w} + \mathbf{w}^T\mathbf{K}^3\mathbf{v} \\ &\quad + \mathbf{w}^T\mathbf{K}^4\mathbf{w} = K^1_{ij} v_i v_j \\ &\quad + K^2_{ij} v_i w_j + K^2_{ji} w_i v_j \\ &\quad + K^4_{ij} w_i w_j = K^1_{ij} v_i v_j \\ &\quad + 2K^2_{ij} v_i w_j + K^4_{ij} w_i w_j, \end{aligned} \quad \text{(C-3)}$$

where we have used the fact that $K^2_{ij} = K^2_{ji}$ (see equation 60). Using the definitions of these matrices, given in equations 15 and 18, we get

$$\begin{aligned} &K^1_{ij} v_i v_j + 2K^2_{ij} v_i w_j + K^4_{ij} w_i w_j \\ &\quad = \alpha^2 \int_\Omega (\phi_{i,x} v_i)^2 \, dx \, dz \\ &\qquad + \beta^2 \int_\Omega (\phi_{i,z} v_i)^2 \, dx \, dz \\ &\qquad + 2(\alpha^2 - \beta^2) \int_\Omega \phi_{i,x} v_i \phi_{j,z} w_j \, dx \, dz \\ &\qquad + \beta^2 \int_\Omega (\phi_{j,x} w_j)^2 \, dx \, dz \\ &\qquad + \alpha^2 \int_\Omega (\phi_{j,z} w_j)^2 \, dx \, dz \\ &\quad = \alpha^2 \int_\Omega (\phi_{i,x} v_i + \phi_{j,z} w_j)^2 \, dx \, dz \\ &\qquad + \beta^2 \int_\Omega (\phi_{i,z} v_i - \phi_{j,x} w_j)^2 \, dx \, dz, \end{aligned} \quad \text{(C-4)}$$

where we have used the fact that

$$\int_\Omega \phi_{i,x} \phi_{j,z} \, dx \, dz = \int_\Omega \phi_{i,z} \phi_{j,x} \, dx \, dz. \quad \text{(C-5)}$$

Clearly, equation C-4 is greater than or equal to zero for any v and w; therefore the matrix on the right-hand side is symmetric positive definite. This completes the proof.

REFERENCES

Alford, R. M., K. R. Kelly, and D. M. Boore, 1974, Accuracy of finite-difference modeling of the acoustic wave equation: Geophysics, **39**, 834–842.

Alterman, Z. S. and F. C. Karal, 1968, Propagation of elastic waves in layered media by finite difference methods: Bulletin of the Seismological Society of America, **58**, 367–398.

Brenner, S. C., and L. R. Scott, 2002, The mathematical theory of finite element methods. Texts in Applied Mathematics: Springer.

Carcione, J. M., G. C. Hermanz, and A. P. E. ten Kroode, 2002, Seismic modeling: Geophysics, **67**, 1304–1325.

Chaljub, E., D. Komatitsch, J.-P. Vilotte, Y. Capdeville, B. Valette, and G. Festa, 2007, Spectral element analysis in seismology, *in* R.-S. Wu and V. Maupin, eds., Advances in wave propagation in heterogeneous media: Advances in Geophysics, 48, Elsevier, 365–419.

Cohen, G., 2002, Higher-order numerical methods for transient wave equations. Scientific Computation: Springer-Verlag.

Cohen, G., and S. Fauqueux, 2000, Mixed finite elements with mass-lumping for the transient wave equation: Journal of Computational Acoustics, **8**, 171–188.

Cohen, G., P. Joly, and N. Tordjman, 1994, Eléments finis d'ordre élevé avec condensation de masse pour l'équation des ondes en dimension 1. Rapport de Recherche 2323, INRIA.

Dormy, E., and A. Tarantola, 1995, Numerical simulation of elastic wave propagation using a finite volume method: Journal of Geophysical Research, **100**, 2123–2134.

Dumbser, M., and M. Kaser, 2006, An arbitrary high-order discontinuous Galerkin method for elastic waves on unstructured meshes – II. The three-dimensional isotropic case: Geophysical Journal International, **167**, 319–336.

Emerman, S. H., W. Schmidt, and R. A. Stephen, 1982, An implicit finite-dif-

ference formulation of the elastic wave equation: Geophysics, **47**, 1521–1526.
Fauqueux, S., 2003, Eléments finis mixtes spectraux et couches absorbantes parfaitement adaptées pour la propagation d'ondes élastiques en régime transitoire: Ph.D. thesis, Université de Paris, IX-Dauphine.
Graves, R. W., 1996, Simulating seismic wave propagation in 3D elastic media using staggered-grid finite differences: Bulletin of the Seismological Society of America, **86**, 1091–1106.
Hughes, T., 1987, The finite element method. Linear static and dynamic finite element analysis: Prentice-Hall International, Inc.
Jenkins, E. W., B. Riviere, and M. F. Wheeler, 2002, A priori error estimates for mixed finite element approximations of the acoustic wave equation: SIAM Journal on Numerical Analysis, **40**, 1698–1715.
Kaser, M., and M. Dumbser, 2006, An arbitrary high-order discontinuous Galerkin method for elastic waves on unstructured meshes - I. The two-dimensional isotropic case with external source terms: Geophysical Journal International, **166**, 855–877.
Kaser, M., M. Dumbser, J. de la Puente, and H. Igel, 2007, An arbitrary high-order discontinuous Galerkin method for elastic waves on unstructured meshes – III. Viscoelastic attenuation: Geophysical Journal International, **168**, 224–242.
Kelly, K. R., R. W. Ward, S. Treitel, and R. M. Alford, 1976, Synthetic seismograms - A finite-difference approach: Geophysics, **41**, 2–27.
Komatitsch, D., J. Ritsema, and J. Tromp, 2002, The spectral-element method, Beowulf computing, and global seismology: Science, **298**, 1737–1742.
Komatitsch, D., and J. Tromp, 1999, Introduction to the spectral element method for three-dimensional seismic wave propagation: Geophysical Journal International, **139**, 806–822.
Komatitsch, D., S. Tsuboi, and J. Tromp, 2005, The spectral-element method in seismology: Geophysical Monograph, **157**, 205–227.
Komatitsch, D., and J. P. Vilotte, 1998, The spectral-element method: an efficient tool to simulate the seismic response of 2D and 3D geological structures: Bulletin of the Seismological Society of America, **88**, 368–392.
Levander, A. R., 1988, Fourth-order finite-difference P-SV seismograms: Geophysics, **53**, 1425–1436.
Lysmer, J., and L. A. Drake, 1972, A finite element method for seismology, *in* Methods in Computational Physics, Volume **11**, Academic Press, 181–216.
Madariaga, R., 1976, Dynamics of an expanding circular fault: Bulletin of the Seismological Society of America, **66**, 639–666.
Marfurt, K. J., 1984, Accuracy of finite-difference and finite-element modeling of the scalar and elastic wave equations: Geophysics, **49**, 533–549.
——–, 1990, Analysys of higher order finite element methods, *in* K. R. Kelly and K. J. Marfurt, ed., Numerical modeling of seismic wave propagation, SEG, 516–520.
Mercerat, D., J. P. Ampuero, and T. Nissen-Meyer, 2006, Dispersion analysis and high-order symplectic time schemes in spectral-element based seismic wave propagation: Eos Transactions American Geophysical Union, **87**, Fall Meeting Supplement, Abstract S41B–1336.
Minkoff, S. E., 2002, Spatial parallelism of a 3D finite difference velocity-stress elastic wave propagation code: SIAM Journal on Scientific Computing, **24**, 1–19.
Mitchell, A., and D. Griffiths, 1980, The finite difference method in partial differential equations: John Wiley and Sons.
Moczo, P., J. Kristek, and E. Bystricky, 2000a, Stability and grid dispersion of the P-SV 4^{th}-order staggered-grid finite-difference scheme: Studia Geophisics et Geodetica, **44**, 381–402.
Moczo, P., J. Kristek, and L. Halada, 2000b, 3D fourth-order staggered-grid finite-difference schemes: Stability and grid dispersion: Bulletin of the Seismological Society of America, **90**, 587–603.
Mulder, W. A., 1999, Spurious modes in finite-element discretizations of the wave equation may not be all that bad: Applied Numerical Mathematics, **30**, 425–445.
Mullen, R., and T. Belytschko, 1982, Dispersion analysis of finite element semidiscretizations of the two-dimensional wave equation: International Journal for Numerical Methods in Engineering, **18**, 11–29.
Patera, A. T., 1984, A spectral element method for fluid dynamics: Laminar flow in a channel expansion: Journal of Computational Physics, **54**, 468–488.
Seriani, G., and E. Priolo, 1994, Spectral element method for acoustic wave simulation in heterogeneous media: Finite Element in Analysis and Design, **16**, 337–348.
Tordjman, N., 1995, Eléments finis d'ordre élevé avec condensation de masse pour l'équation des ondes: Ph.D. thesis, Université de Paris, IX-Dauphine.
Virieux, J., 1984, SH-wave propagation in heterogeneous media — Velocity-stress finite-difference method: Geophysics, **49**, 1933–1942.
——–, 1986, P-SV wave propagation in heterogeneous media — Velocity-stress finite-difference method: Geophysics, **51**, 889–901.
Watkins, D. S., 2002, Fundamentals of matrix computations. Pure and Applied Mathematics, 2nd ed.: John Wiley and Sons.